SCaMC-1 promotes cancer cell survival by desensitizing mitochondrial permeability transition through ATP/ADP mediated matrix Ca^{2+} buffering

Javier Traba[1,2], Araceli del Arco[3], Michael R. Duchen[2], Gyorgy Szabadkai[2†*] and Jorgina Satrústegui[1†*]

[1] *Departamento de Biología Molecular, Centro de Biología Molecular Severo Ochoa UAM-CSIC, CIBER de Enfermedades Raras (CIBERER), Universidad Autónoma, Madrid, Spain.*

[2] *Department of Cell and Developmental Biology, UCL Consortium for Mitochondrial Research, University College London, Gower Street, London WC1E 6BT, UK.*

[3] *Área de Bioquímica, Centro Regional de Investigaciones Biomédicas (CRIB), Facultad de Ciencias Ambientales y Bioquímica, Universidad de Castilla-La Mancha, Toledo, Spain.*

[†]*These authors share senior authorship*

[*] *Correspondence to:*

Jorgina Satrústegui

Tel: 034-911964621; Fax: 034-911964420; E-mail: jsatrustegui@cbm.uam.es

Gyorgy Szabadkai

Tel: 44 02076797362; Fax: 44 02076794561; E-mail: g.szabadkai@ucl.ac.uk

Running title: The ATP-Mg/Pi carrier SCaMC-1 regulates mPT

ABSTRACT

Ca^{2+} mediated mitochondrial permeability transition (mPT) is the final common pathway of stress-induced cell death in many major pathologies, but its regulation in intact cells is poorly understood. Here we report that the mitochondrial carrier SCaMC-1/SLC25A24 mediates ATP-Mg^{2-}/Pi^{2-} and/or $HADP^{2-}$/Pi^{2-} uptake into the mitochondria following cytosolic [Ca^{2+}] rises. ATP and ADP contribute to Ca^{2+} buffering in the mitochondrial matrix, resulting in desensitization of the mPT. Comprehensive gene expression analysis showed that SCaMC-1 overexpression is a general feature of transformed and cancer cells. The knockdown of the transporter led to vast reduction of mitochondrial Ca^{2+} buffering capacity and sensitized cells to mPT mediated necrotic death triggered by oxidative stress and Ca^{2+} overload. These findings revealed that SCaMC-1 exerts a negative feedback control between cellular Ca^{2+} overload and mPT dependent cell death, also suggesting that the carrier might represent a novel target for cancer therapy.

Keywords: adenine nucleotides / ATP-Mg/Pi carrier / calcium / mitochondria / permeability transition pore / oxidative stress / cell death / cancer

Abbreviations: $[Ca^{2+}]_{cyt}$, cytosolic [Ca^{2+}]; $[Ca^{2+}]_m$, mitochondrial [Ca^{2+}]; ANT, adenine nucleotide translocator; BKA, bongkrekic acid; CAT, carboxyatractyloside; CRC, Ca^{2+} retention capacity; CsA, cyclosporin A; CyP-D, cyclophilin D; cytAEQ, cytosolic aequorin; ER, endoplasmic reticulum; IC, intracellular; IMM, inner mitochondrial membrane; IP_3, inositol 1,4,5 trisphosphate; MCU, mitochondrial Ca^{2+} uniporter; mPT, mitochondrial permeability transition; mPTP, mitochondrial permeability transition pore; mtAEQmut, low affinity mitochondrial aequorin; mtAEQwt, mitochondrial aequorin; RR, ruthenium red; ROS, reactive oxygen species; VDAC, voltage dependent anion channel; $\Delta\Psi$, mitochondrial membrane potential.

INTRODUCTION

ATP generation by aerobic glycolysis is indispensable for the survival and proliferation of many tumour cell types, associated with resistance to stress induced apoptotic and necrotic death.[1,2] In many cell death models, mPT plays a central role in permeabilizing the inner mitochondrial membrane (IMM), leading to necrotic cell death.[3] The mPT is triggered by the formation of a large (cutoff ~1.5 kD), non-specific pore (mPTP) in the IMM under conditions of Ca^{2+} overload and/or oxidative stress. mPTP opening dissipates the mitochondrial membrane potential ($\Delta\Psi$) and can be associated with mitochondrial swelling, particularly under *in vitro* conditions.[4] Although the molecular composition of the mPTP is still debated, pharmacological and genetic evidence strongly supports its implication in cell death in a wide range of pathologies.[5] Accordingly, the resistance of tumour cells to death could be explained by decreased probability of mPTP opening. Indeed, it has been suggested that Bcl-2 overexpression or reduction of Bax/Bak expression can mediate protective effect by diminishing mitochondrial Ca^{2+} load from the endoplasmic reticulum (ER) Ca^{2+} store.[6] In addition, direct modification of putative mPTP components, such as hexokinase II binding to the VDAC[7] and dephosphorylation of cyclophilin D (CyP-D)[8] have also been shown to reduce the sensitivity of mPTP formation to elevations of $[Ca^{2+}]_m$. However, modification of the mPT is not essential for mediating cancer cell protection,[9] and no intrinsic mitochondrial factor has been described so far contributing to the development of resistance to mPT in cancer cells.

The net mitochondrial content of adenine nucleotides is central to the regulation of Ca^{2+} induced mPT in isolated organelles, but the underlying mechanisms remained unclear.[10] The adenine nucleotide translocator (ANT) of the IMM exchanges ATP^{4-} for ADP^{3-}, but does not change the total matrix ATP/ADP/AMP content. The net content of adenine nucleotides may rather be determined by the ATP-Mg/Pi transporter, which mediates a reversible, electroneutral exchange of $ATP\text{-}Mg^{2-}$ or $HADP^{2-}$ for HPO_4^{2-}, stimulated by extramitochondrial Ca^{2+}.[11] Recently, the genes encoding this transporter have been identified. There are four paralogues in mammals, SCaMC-1/SLC25A24, SCaMC-2/SLC25A25, SCaMC-3/SLC25A23 and SCaMC-3-like/SLC25A41.[12,13] The transporter consists of a C-terminal domain comprising 6 transmembrane helices homologous to the mitochondrial carrier proteins,[14] and an N-terminal domain with Ca^{2+} binding EF hands,[15] which confers Ca^{2+} sensitivity to the carrier.[11,16] These properties of the carrier prompted us to investigate the role it might play in regulating Ca^{2+} retention capacity (CRC) of mitochondria and mPTP formation in intact cells.

Here we report that SCaMC-1 is the dominant isoform of the ATP-Mg/Pi carrier in cancer cells and highly overexpressed in a series of *in vivo* tumours and cell lines. We found that cytosolic Ca^{2+} mediated uptake of ATP/ADP by SCaMC-1 increases intramitochondrial Ca^{2+} buffering, and thus contributes to the resistance to mPT in tumour cells.

RESULTS AND DISCUSSION

SCaMC-1 is highly expressed in tumours and cancer cell lines, and mediates Ca^{2+} dependent ATP-Mg and ADP uptake into mitochondria

First, using western blot, immunofluorescence and *in silico* approaches we showed that SCaMC-1 is the dominant and highly expressed isoform of ATP-Mg/Pi carrier family in a wide range of tumours, cancer cell lines and highly proliferative immortalized cells (Fig. 1A-C, Fig. S1). Therefore, in order to study the role of SCaMC-1 in mitochondrial adenine nucleotide transport and cancer cell fate, we generated stable SCaMC-1-*knock-down* cell lines using COS-7 and 143B parental lines (Fig. 1D-G). In the SCaMC-1-*knock-down* (SCaMC-1-KD) COS-7 and 143B clones, the expression was reduced to 29.6 ± 3.8% and 41.7 ± 5.0%, respectively (Fig. 1F).

Next, in order to evaluate mitochondrial adenine nucleotide transport in the parental and SCaMC-1-KD clones, cells were transiently or stably transfected with mitochondrial matrix targeted luciferase to measure mitochondrial ATP levels in digitonin-permeabilized cells or isolated mitochondria.[17] Following cell permeabilization in an intracellular (IC) buffer supplemented with luciferin, added ATP was imported into the mitochondria (Fig. 2). Under Ca^{2+} free conditions the uptake of ATP was completely inhibited by 10 μM carboxyatractyloside (CAT), indicating that it was mediated entirely by ATP/ADP exchange through ANT. Ca^{2+}-independent ATP import was identical in parental and SCaMC-1-KD cells (Fig. 2A). However, in the presence of 100 μM Ca^{2+}, ATP was rapidly imported into the mitochondrial matrix even in the presence of CAT (Fig. 2B). The transport was activated by extramitochondrial Ca^{2+}, as 200 nM ruthenium red (RR) was present in all the experiments to prevent Ca^{2+} uptake through the mitochondrial Ca^{2+} uniporter (MCU). Under these conditions, ADP uptake was also observed, as measured after its conversion to ATP due to oxidative phosphorylation in the matrix (Fig. 2C, Fig. S2A)[16]. Chelation of Mg^{2+} (with 1 mM EDTA) reduced ATP uptake rate (not shown). The dependence of CAT-insensitive ATP transport on extramitochondrial [Ca^{2+}] was determined on isolated mitochondria using a mitochondrial luciferase expressing COS-7 cell line, showing a half maximal activation at [Ca^{2+}] = 12.7 ± 5.3 μM (Fig. 2D,F). Pi addition reversed the activity of the transporter (Fig. 2E), with a similar Ca^{2+} dependence. These results confirmed that these cells express a *bona fide* Ca^{2+}-dependent ATP-Mg/Pi carrier, mediating the exchange of ATP-Mg and free ADP to Pi.[18]

Importantly, the CAT-insensitive/Ca^{2+}-dependent ATP-Mg/ADP transport was strongly reduced in SCaMC-1-KD cells (Fig. 2B,C; ATP: to 56 ± 8%, ADP: to 55 ± 5% of the control rate) to an extent similar to the reduction of SCaMC-1 expression, demonstrating that SCaMC-1 mediates ATP-Mg/Pi transporter activity facilitated by extramitochondrial [Ca^{2+}].

SCaMC-1 protects cancer cells from oxidative stress induced death

High expression levels of SCaMC-1 in tumours and cancer cell lines suggested that the carrier confers selective advantage to proliferation either by altering cellular metabolism, or by mediating protection against cell death. We observed no effect on cellular energy metabolism and proliferation (see Fig. S3). Thus next, in order to test whether SCaMC-1 plays a role in modulating cell death pathways, control and SCaMC-1-KD were exposed to (i) oxidative stress by H_2O_2 or menadione treatment, leading to mitochondrial Ca^{2+} overload, mPT and necrosis or (ii) staurosporine, triggering the intrinsic pathway of apoptosis. As shown in Fig. 3A-C, reduced expression of SCaMC-1 rendered cells more susceptible to oxidative stress induced cell death (Fig. 3A,B), while had no effect on apoptosis induced by staurosporine (Fig. 3C, Fig. S4A). These data indicated that high expression levels of SCaMC-1 confer resistance specifically to mPT-dependent cell death.

In order to directly demonstrate the effect of SCaMC-1 silencing on mPT in intact cells, we studied Ca^{2+} and reactive oxygen species (ROS) mediated mitochondrial depolarization using confocal microscopy, and a previously established model of phototoxicity.[19] Following TMRM loading, cells were illuminated with high laser power, which leads to the local generation of ROS in the mitochondria. ROS mediated Ca^{2+} release from the ER results in mitochondrial Ca^{2+} overload and mPT, visualized by the loss of TMRM. As shown on Fig. 3D, illumination of parental COS-7 cells had no effect on $\Delta\Psi_m$, while it led to the complete loss of $\Delta\Psi_m$ in SCaMC-1-KD cells. The effect was Ca^{2+} dependent, since it was completely prevented by in Ca^{2+}-free medium (in the presence of 100 μM EGTA) and by depleting the internal Ca^{2+} stores with thapsigargin (1 μM). Moreover, the addition of cyclosporin A (CsA) and bongkrekic acid (BKA), inhibitors of mPT,[20] prevented mitochondrial depolarization in SCaMC-1-KD cells, confirming that it was indeed due to mPT.

Finally, to test whether the high level of SCaMC-1 expression is indeed responsible for protection against mPT-dependent cell death, we (i) rescued the expression of SCaMC-1 in SCaMC-1-KD 143B cells, using a mutant cDNA containing synonymous mutations (SCaMC-1*), and (ii) overexpressed the protein in liver clone 9 cells with low levels of endogenous SCaMC-1 (Fig. S1). Re-expression of SCaMC-1 in SCaMC-1-KD 143B cells (Fig. 3E), as well as its overexpression in both a transient (Fig. 3E) or stable (Fig. 3F) manner in clone 9 cells rendered cells more resistant to H_2O_2 or C_2-ceramide induced cell death.[21] These results confirmed that SCaMC-1 mediates protection against mPT induced cell death.

SCaMC-1 mediated ATP/ADP uptake controls mitochondrial Ca^{2+} buffering capacity

Elevation of the mitochondrial matrix free [Ca^{2+}] is the most potent inducer of mPT. To determine the effect of SCaMC-1 on cellular and mitochondrial Ca^{2+} handling in intact cells, we measured agonist-evoked cytosolic and mitochondrial Ca^{2+} transients in cells transiently transfected with a cytosolic aequorin (cytAEQ) or a mitochondrial aequorin (mtAEQwt) probe, respectively.[22]

After reconstitution of the probe with the aequorin cofactor coelenterazine, COS-7 cells were stimulated with 100 μM ATP, an agonist acting on G-protein-coupled receptors and leading to the production of IP_3. The consequent Ca^{2+} release from the intracellular stores induced a cytosolic Ca^{2+} transient, which was identical in control and SCaMC-1-KD cells (Fig. 4A, left panel). However, intriguingly, mitochondrial Ca^{2+} uptake was increased almost three times in SCaMC-1-KD cells as compared to controls (Fig. 4B, left panel). Similar results were obtained when parental and SCaMC-1-KD 143B cells were stimulated with 100 μM histamine (Fig. 4A,B, right panels).

Mitochondrial free [Ca^{2+}] is determined by the balance between Ca^{2+} influx into and Ca^{2+} extrusion from the organelle, as well as by Ca^{2+} buffering in the matrix. Thus, in order to characterize the mechanism by which SCaMC-1 activity affects $[Ca^{2+}]_m$, we determined mitochondrial Ca^{2+} influx and efflux rates in isolated mitochondria or permeabilized cells. When measured in the mitochondrial matrix in permeabilized cells expressing the low affinity mitochondrially targeted aequorin probe (mtAEQmut), the addition of the same amount of extramitochondrial Ca^{2+} (10 μM) caused significantly greater elevation in $[Ca^{2+}]_m$ in both COS-7 and 143B SCaMC-1-KD cells as compared to their parental counterpart (Fig. 4C). However, when measured in the extramitochondrial space with the fluorescent Ca^{2+} sensitive dye Calcium-Green, mitochondria from both the parental and SCaMC-1-KD cells took up the same amount of Ca^{2+} with the same rate (Fig. 4D). Ca^{2+} efflux was measured after inhibition of Ca^{2+} uptake with RR. In that situation, the rate of Ca^{2+} efflux depends only on the matrix free [Ca^{2+}]. After loading 143B mitochondria with Ca^{2+} in the presence of 1 mM ATP-Mg, RR was added. Fig. 4E shows that the efflux of Ca^{2+} (both Na^+-independent and Na^+-dependent) was more rapid in SCaMC-1-KD mitochondria than in controls, indicating (i) higher free [Ca^{2+}] following Ca^{2+} load in mitochondria lacking SCaMC-1 mediated ATP uptake, and (ii) normal activity of the efflux machineries. These results show that increased $[Ca^{2+}]_m$ in the mitochondria of SCaMC-1-KD cells is not the consequence of increased Ca^{2+} uptake or reduced Ca^{2+} efflux, but rather reflects reduced Ca^{2+} buffering capacity in the matrix.

Ca^{2+} buffering in the mitochondrial matrix is principally achieved by the formation of insoluble Ca^{2+}-Pi precipitates.[23] A higher level of Ca^{2+} precipitation in control mitochondria could be explained if the adenine nucleotides transported by SCaMC-1 facilitate the precipitation of Ca^{2+} and Pi in the matrix, as has been suggested previously.[24] The formation of Ca^{2+}-Pi precipitates can be measured by the apparent mitochondrial contraction (an increase in

light scattering measured as absorbance at 540 nm) immediately following Ca^{2+} uptake.[23,25] Indeed, mitochondria of 143B cells displayed apparent contraction when Ca^{2+} was added to the medium, which was inhibited by the addition of RR, preventing Ca^{2+} entry through the MCU. Moreover, the initial increase in absorbance in the presence of ATP-Mg was significantly higher in the mitochondria of control than that of SCaMC-1-KD 143B cells (0.041 ± 0.006 absorbance units per min compared to 0.018 ± 0.003, respectively mean ± SEM, n=3, p = 0.048; not shown). These results suggest higher efficiency of Ca^{2+}-Pi precipitate mediated Ca^{2+} buffering in the presence of SCaMC-1.

SCaMC-1 increases mitochondrial Ca^{2+} retention capacity and reduces probability of Ca^{2+} mediated mPTP opening

Regulation of Ca^{2+}-dependent mPTP opening by low micromolar concentrations of ATP/ADP is well established,[26] and is mediated by a nucleotide induced switch in the conformation of ANT. However, higher concentrations of adenine nucleotides, in the physiological millimolar range, are also able to prevent mPTP formation.[27] Thus we tested whether Ca^{2+} mediated uptake of ATP-Mg/ADP by SCaMC-1 can affect mitochondrial CRC, a measure of the amount of Ca^{2+} required in order to trigger mPT.

CRC was studied by monitoring Ca^{2+} uptake into mitochondria using Calcium-Green to measure [Ca^{2+}] in the buffer. Permeabilized cells were treated with sequential Ca^{2+} pulses, and Ca^{2+} uptake into mitochondria was measured as a drop in the fluorescence. mPTP opening was detected as a steady increase of fluorescence due to Ca^{2+} release from mitochondria. Other organelles, such as the ER do not contribute significantly to Ca^{2+} uptake, as RR completely inhibited uptake (not shown). As summarized in Fig. 5A, permeabilized control and SCaMC-1-KD COS-7 cells display a similar mitochondrial CRC both in the absence of adenine nucleotides and in the presence of low ADP (100 μM). In both lines, 100 μM ADP increased the CRC only slightly (less than 10 % on COS-7 cells, $p>0.05$; 20% in 143B cells, $p<0.05$, not shown), probably by interacting with the ANT and triggering the 'm' conformation of the carrier, as previously demonstrated in liver and brain mitochondria.[20] Most importantly, however, in the presence of 1 mM ATP or 2 mM ADP, control COS-7 or 143B cells displayed a pronounced increase in the threshold for mPTP opening compared to SCaMC-1-KD cells, whose CRC was practically identical to that measured in the presence of 100 μM ADP. The presence of Mg^{2+} was essential for the protective effect of ATP, but not for that of ADP, consistently with the substrate specificity of SCaMC-1. The same results were obtained in isolated mitochondria from COS-7 or 143B cells (Fig. 5B,C), as mitochondria from control cells are able to take up more Ca^{2+} in the presence of 1 mM ATP or 2 mM ADP than SCaMC-1-KD mitochondria before release of accumulated Ca^{2+} by mPTP opening.

mPTP opening can also be studied by monitoring mitochondrial swelling. Fig. 5D shows that Ca^{2+} addition to COS-7 mitochondria in the presence of ATP initially caused contraction, while further additions led to swelling (a decrease in absorbance). The number of Ca^{2+} additions needed to trigger swelling in the presence of 2 mM ATP was always higher in control mitochondria as compared to SCaMC-1-KD mitochondria. On the other hand, swelling was identical in the absence of nucleotides. Similar results were obtained in 143B isolated mitochondria (Fig. 5E).

In the presence of 5 μM CsA, an inhibitor of mPT, the CRC was enhanced in permeabilized cells and isolated COS-7 mitochondria (Fig. 5A,B), and mitochondrial swelling was inhibited (Fig. 5D), demonstrating that the effects observed were due to mPTP opening. CsA produced these effects in both control and SCaMC-1-KD mitochondria, but the differences between both lines in the presence of 1 mM ATP were still observed. On the other hand, 5 μM CAT, a stimulator of mPT, greatly reduced the CRC in both control and SCaMC-1-KD permeabilized cells, but a difference between the two cell lines in the presence of 1 mM ATP was still observed (Fig. 5A). The increase in CRC by 1 mM ATP in the presence of CAT in control cells proves that the effect of high concentrations of adenine nucleotides was indeed independent of the ANT, as had been suggested previously.[26] Furthermore, in the presence of 5 μM BKA, another ANT inhibitor, the differences between both lines obtained at 1 mM ATP were still present (Fig. 5A).

Interestingly, 143B permeabilized cells and isolated mitochondria were largely unaffected by CsA (Fig. 5C, Fig. S4B). This is not due to a lower expression of CyP-D (Fig. 1E), the regulatory component of the pore that is targeted by CsA, an argument which is used to explain the CsA-insensibility of brain mitochondria.[28] An alternative explanation is that 143B are tumour cells, whereas COS-7 are merely immortalized cells. Tumour cells display a constitutive activation of the ERK pathway, which has been suggested to dephosphorylate and inactivate CyP-D,[8] and thus, although present, CyP-D may be inactive in 143B mitochondria. In order to study this possibility first the phosphorylation state of CyP-D was assayed by the Mn^{2+}-Phos-tag SDS-PAGE technique. In FLAG-CyP-D overexpressing COS-7 cells, several shifted CyP-D bands were observed, demonstrating the phosphorylated status of the protein (Fig. 5F). Importantly, these bands were almost completely missing in FLAG-CyP-D overexpressing 143B cells in spite of the equal expression of CyP-D. In addition, 143B cells showed a constitutive phosphorylation of ERK, whereas COS-7 cells did not (Fig. 5F). In this pathway, ERK was shown to phosphorylate and inactivate GSK-3β, the putative CyP-D kinase. Indeed, we found that that GSK-3β was phosphorylated in 143B cells, but not in COS-7 cells (Fig. 5F). These results suggest that in 143B cells, as a result of a constitutively active ERK/GSK-3β pathway, CyP-D is mostly dephosphorylated and thus inactive. Conversely, in COS-7 cells CyP-D is partially phosphorylated and active due to the lack of ERK activation.

In summary, these results provide evidence that adenine nucleotides regulate mPTP opening independently of the ANT, via a lower affinity site, reflecting the activity of the ATP-Mg/Pi carrier. The modification of the mitochondrial adenine nucleotide content by the ATP-Mg/Pi carrier regulates the CRC and mPTP opening, probably by modifying the formation of Ca^{2+}-Pi precipitates and thus altering the Ca^{2+} buffering capacity of the mitochondrial matrix.

CONCLUDING REMARKS

Altogether, our data fully support a model where SCaMC-1 is responsible for a cytoprotective mechanism by mediating (i) ATP/ADP uptake in the mitochondrial matrix, triggered by increases of $[Ca^{2+}]_{cyt}$; (ii) increased mitochondrial Ca^{2+} buffering capacity due to elevated adenine nucleotide levels; (iii) desensitization of Ca^{2+} mediated mPT. This pathway represents a novel mechanism promoting cancer cell survival under stress conditions.

High levels of SCaMC-1 were previously found by screening approaches in colorectal carcinomas,[29] breast cancer[30] and in several cancer cell lines.[15,31] Our *in silico* studies confirmed and extended these findings to 67 different tumour types where SCaMC-1 expression significantly exceeded its expression in their normal tissue counterpart. Importantly, this pattern was specific to the SCaMC-1 isoform, which has an order of magnitude higher transport activity than SCaMC-3.[18] This suggested that the benefit conferred by SCaMC-1 overexpression implies a high rate of transport of adenine nucleotides in the mitochondrial matrix under conditions of pathologically elevated $[Ca^{2+}]_{cyt}$. The $S_{0.5}$ for Ca^{2+} of SCaMC-1 was found to be 12.7 μM, adequate to respond to changes in the $[Ca^{2+}]_{cyt}$ that are transmitted to the mitochondria through the MCU during Ca^{2+} overload both under physiological and pathological conditions. Indeed, SCaMC-1 expression was not essential for cellular proliferation, rather was required for protection against oxidative stress and Ca^{2+} overload induced cell death. This resembles the effect of Bcl-2 overexpression,[32] Bax and Bak downregulation,[6] Bad phosphorylation,[33] hexokinase II binding to mitochondria[7] and the constitutive activation of the ERK pathway.[8] Distinct from some of these studies, however, is that the role of SCaMC-1 was exclusive to mPT driven cell death, since no effect was observed on cell death induced by staurosporine. Altogether, the selective overexpression of SCaMC-1 over normal tissues and its specific role in protecting from oxidative stress induced cell death indicate that selective ablation of SCaMC-1 function might represent a novel strategy to abolish tumour growth in a wide range of cancers.

Low concentrations of adenine nucleotides (≈ 100 μM) inhibit mPTP opening in isolated liver and brain mitochondria,[26] most likely by conformational changes triggered by binding to high affinity sites (Kd ≈ 5 - 10 μM) of the ANT.[20] However, adenine nucleotides in the millimolar, physiological range also exhibit potent mPT inhibiton, even in the presence of ANT inhibitors.[10,27,34] The site of this ANT-independent protection remained unexplained.[35] Here we

found that SCaMC-1, which displays binding sites for adenine nucleotides in this affinity range (Kd ≈ 0.2 - 0.5 mM) is able to mediate this effect.

While the mechanism by which matrix adenine nucleotides protect from mPT is not completely understood, our data clearly suggest that altered mitochondrial Ca^{2+} handling plays a major role in the effect. The lack of ATP/ADP uptake in the mitochondria of SCaMC-1-KD cells led to a vast increase of free matrix [Ca^{2+}] following activation of cellular Ca^{2+} signalling pathways, as compared to cells with high SCaMC-1 expression levels.

Accordingly, we propose that the SCaMC-1 mediated adenine nucleotide load in the mitochondrion buffers matrix free [Ca^{2+}], preventing mitochondrial Ca^{2+} overload during oxidative stress and preventing mPT induction. As a major route of mitochondrial Ca^{2+} buffering, Ca^{2+} and Pi form amorphous $Ca_3(PO_4)_2$ precipitates in the matrix.[23,25] It has long been suggested that the presence of adenine nucleotides in the mitochondrial matrix is essential for this process, either by stabilizing the Ca^{2+}-Pi deposits or by priming their precipitation.[24] As a result, mitochondrial Ca^{2+}-Pi precipitates contain adenine nucleotides,[36] and ATP may account for as much as 7 % of the dry weight of some Ca^{2+}-Pi precipitates.[37] Interestingly, Ca^{2+}-Pi precipitates in isolated mitochondria also contain Mg^{2+} when Ca^{2+} loading was performed in the presence of ATP, but not in the presence of ADP,[25] which matches the substrate specificity of the ATP-Mg/Pi carriers.[11,18]

The protective effect of increasing amounts of matrix Ca^{2+}-Pi precipitates has already been observed, particularly in cell death models mediated entirely by Ca^{2+} overload, such as glutamate excitotoxicity in primary neurons.[38] Our findings extend these observations to cancer cells, and provide direct demonstration of the effect of SCaMC-1 *knock-down* mediated adenine nucleotide depletion on mitochondrial Ca^{2+} handling.

EXPERIMENTAL PROCEDURES

Cell culture, transfection, generation of SCaMC-1-KD and mitochondrial luciferase expressing clones

COS-7 cells, liver clone 9 cells and 143B osteosarcoma cells were cultured in Dulbecco's modified Eagle's medium supplemented with 5 % inactivated fetal bovine serum (Invitrogen) at 37 °C in a 5 % CO_2 atmosphere. For transfections, the LipofectAMINE reagent (Invitrogen) was used as previously described.[15] Details of the constructs and generation of SCaMC-1-KD clones, cells overexpressing SCaMC-1 or cells stably expressing mitochondrially targeted luciferase are described in the Supplementary Methods section.

Immunofluorescence and western blotting

Immunofluorescent stainings were performed as described previously.[15] Anti-SCaMC-1 antibodies were diluted 1:400. Fluorescence microscopy was performed using an Axiovert epifluorescence microscope (Carl Zeiss) at a nominal magnification of X100.

For western blotting, total homogenates and mitochondrial-enriched fractions were obtained from cells and mouse tissues as described[15] and analyzed by western blotting (for details see Supplementary Methods). To determine the phoshorylation status of CyP-D, Mn^{2+}-Phos-tag SDS-PAGE was performed[39]. Poly-acrylamide gels were supplemented with 200 μM $MnCl_2$ and the Phos-tag reagent (Nard Institute, Japan). Phosphorylated proteins bind to the Phos-tag, and thus are delayed in the gel and separated from unphosphorylated proteins. After electrophoresis, the gels were washed with transfer buffer containing 1 mM EDTA and then with transfer buffer without EDTA according to the manufacturer's protocol, before transfer to PVDF membranes. Membranes were probed with CyP-D antibodies.

Measurements of mitochondrial Ca^{2+} uptake and swelling on isolated mitochondria or permeabilized cells

Mitochondria were isolated by homogenization and differential centrifugation according to standard protocols. Mitochondrial Ca^{2+} uptake was measured in the presence of the Ca^{2+}-sensitive fluorescent probe Calcium-Green 5N (0.1 μM, excitation 506 nm, emission 532 nm) using digitonin-permeabilized cells or isolated mitochondria (for details see Supplementary Methods).

Measurement of cellular respiration and $\Delta\Psi_m$

Cell respiration was measured using a Seahorse XF24 Extracellular Flux Analyzer (Seahorse Bioscience, Billerica, MA, USA; for details see Supplementary Methods). $\Delta\Psi_m$ was measured with the fluorescent lipophilic cationic dye tetramethylrhodamine methyl ester (TMRM). Cells

were stained with 200 nM TMRM for 10 min, and red fluorescence was measured by flow cytometry.

10% laser power of the 543 HeNe laser line on the Zeiss 510 confocal system was used to induce mPT, which was detected by the loss of TMRM signal, as previously described.[19] Cells were preincubated with 100 nM TMRM for 20 min at 37 ºC in a modified Krebs-Ringer buffer (KRB; 135 mM NaCl, 5 mM KCl, 1 mM MgSO4, 0.4 mM K_2HPO_4, 1 mM $CaCl_2$, 5.5 mM glucose, 20 mM HEPES, pH 7.4). TMRM was then present throughout the subsequent measurements. Confocal images were obtained using a Zeiss 510 LSM/META system using a x40 oil-immersion objective. For detection a 560-nm long-pass filter was used.

Luminescent detection of cellular [Ca^{2+}] and [ATP]

Cytosolic and mitochondrial [Ca^{2+}] in intact cells was measured 48 hours after transient transfection with cytAEQ and mtAEQwt probes as previously described.[22] To measure mitochondrial ATP levels in permeabilized cells, experiments were carried out 24 h after transient transfection with mitochondrial luciferase.[17] For experimental details see Supplementary Methods.

Cell death detection

Cells were incubated with H_2O_2, menadione or staurosporine for the time periods indicated in the figure legends and cell death was evaluated by previously described methods[5,7,8,21]: (i) by microscopy after loading with 1 μM Calcein-AM to stain alive cells and 2 μM PI to stain the nuclei of dead cells; (ii) by flow cytometry after loading with 2 μM PI to stain the nuclei of dead cells; (iii) by flow cytometry after incubation with 200 nM TMRM to detect mitochondrial depolarization and FITC-conjugated Annexin-V (Sigma) to detect phosphatidylserine exposure on the cell surface and (iv) by flow citometry using the Annexin V-FITC Apoptosis Detection Kit (Sigma).

CONFLICT OF INTEREST

The authors declare no conflict of interest.

ACKNOWLEDGEMENTS

We thank Dr. María Sánchez-Aragó, Dr. Laura Formentini, Laura Sánchez-Cenizo and María Royo for useful help, reagents and comments, Dr. Claudia Castillo for help with data analysis and Alejandro Arandilla for technical assistance. We also thank Dr. Paolo Bernardi and Dr. Andrea Rasola for the supply of plasmid pcDNA3-FLAG-CyP-D. This work was supported by grants from Ministerio de Educación y Ciencia (BFU2008-04084/BMC), Comunidad de Madrid (S-GEN-0269-2006 MITOLAB-CM), European Union (LSHM-CT-2006-518153), CIBERER

(an initiative of the ISCIII) to JS, by grants from the ISCIII (PI080610) to AdelA and by an institutional grant from the Fundación Ramón Areces to the Centro de Biología Molecular Severo Ochoa. GS was supported by Parkinson's UK (G-0905). JT is a recipient of a fellowship from Comunidad de Madrid.

REFERENCES

1) Hanahan D, Weinberg RA. Hallmarks of cancer: the next generation. *Cell* 2011; **144**: 646-674.

2) Kroemer G, Pouyssegur J. Tumor cell metabolism: cancer's Achilles' heel. *Cancer Cell* 2008; **13**: 472-482.

3) Kroemer G, Galluzzi L, Brenner C. Mitochondrial membrane permeabilization in cell death. *Physiol Rev* 2007; **87**: 99-163.

4) Di Lisa F, Bernardi P. Mitochondria and ischemia-reperfusion injury of the heart: fixing a hole. *Cardiovasc Res* 2006; **70**:191-199.

5) Baines CP, Kaiser RA, Purcell NH, Blair NS, Osinska H, Hambleton MA, et al. Loss of cyclophilin D reveals a critical role for mitochondrial permeability transition in cell death. *Nature* 2005; **434**: 658-662.

6) Scorrano L, Oakes SA, Opferman JT, Cheng EH, Sorcinelli MD, Pozzan T, Korsmeyer SJ. BAX and BAK regulation of endoplasmic reticulum Ca2+: a control point for apoptosis. *Science* 2003; **300**: 135-139.

7) Chiara F, Castellaro D, Marin O, Petronilli V, Brusilow WS, Juhaszova M, et al. Hexokinase II detachment from mitochondria triggers apoptosis through the permeability transition pore independent of voltage-dependent anion channels. *PLoS One* 2008; **3**: e1852.

8) Rasola A, Sciacovelli M, Chiara F, Pantica B, Brusilow WS, Bernardi P. Activation of mitochondrial ERK protects cancer cells from death through inhibition of the permeability transition. *Proc Natl Acad Sci USA* 2010; **107**: 726-731.

9) Jones AW, Szabadkai G. Ca^{2+} transfer from the ER to mitochondria: channeling cell death by a tumor suppressor. *Dev Cell* 2011; **19**: 789-90.

10) Zoratti M, Szabò I. The mitochondrial permeability transition. *Biochim Biophys Acta* 1995; **1241**: 139-176.

11) Aprille JR. Mechanism and regulation of the mitochondrial ATP-Mg/P(i) carrier. *J Bioenerg Biomembr* 1993; **25**: 473-481.

12) Satrústegui J, Pardo B, del Arco A. Mitochondrial transporters as novel targets for intracellular calcium signaling. *Physiol Rev* 2007; **87**: 29-67.

13) Traba J, Satrústegui J, del Arco A. Characterization of SCaMC-3-like/slc25a41, a novel calcium-independent mitochondrial ATP-Mg/Pi carrier. *Biochem J* 2009; **418**: 125-33.

14) del Arco A, Satrústegui J. New mitochondrial carriers: an overview. *Cell Mol Life Sci* 2005; **62**: 2204-2227.

15) del Arco A, Satrústegui J. Identification of a novel human subfamily of mitochondrial carriers with calcium-binding domains. *J Biol Chem* 2004; **279**: 24701-24713.

16) Traba J, Froschauer EM, Wiesenberger G, Satrústegui J, del Arco A. Yeast mitochondria import ATP through the calcium-dependent ATP-Mg/Pi carrier Sal1p, and are ATP consumers during aerobic growth in glucose. *Mol Microbiol* 2008; **69**: 570-585.

17) Poncet D, Pauleau AL, Szabadkai G, Vozza A, Scholz SR, Le Bras M, et al. G. Cytopathic effects of the cytomegalovirus-encoded apoptosis inhibitory protein vMIA. *J Cell Biol* 2006; **174**: 985-996.

18) Fiermonte G, De Leonardis F, Todisco S, Palmieri L, Lasorsa FM, Palmieri F. Identification of the mitochondrial ATP-Mg/Pi transporter. Bacterial expression, reconstitution, functional characterization, and tissue distribution. *J Biol Chem* 2004; **279**: 30722-30730.

19) Duchen MR. Mitochondria and Ca(2+)in cell physiology and pathophysiology. *Cell Calcium* 2000; **28**: 339–348.

20) Bernardi P, Krauskopf A, Basso E, Petronilli V, Blachly-Dyson E, Di Lisa F, Forte MA. The mitochondrial permeability transition from in vitro artifact to disease target. *FEBS J* 2006; **273**: 2077-2099.

21) Szabadkai G, Simoni AM, Chami M, Wieckowski MR, Youle RJ, Rizzuto R. Drp-1-dependent division of the mitochondrial network blocks intraorganellar Ca2+ waves and protects against Ca2+-mediated apoptosis. *Mol Cell* 2004; **16**:59-68.

22) Chiesa A, Rapizzi E, Tosello V, Pinton P, de Virgilio M, Fogarty KE, Rizzuto R. Recombinant aequorin and green fluorescent protein as valuable tools in the study of cell signalling. *Biochem J* 2001; **355**: 1-12.

23) Nicholls DG, Chalmers S. The integration of mitochondrial calcium transport and storage. *J Bioenerg Biomembr* 2004; **36**: 277-281.

24) Carafoli E, Rossi CS, Lehninger AL. Uptake of adenine nucleotides by respiring mitochondria during active accumulation of Ca++ and Phosphate. *J Biol Chem* 1965; **240**: 2254-2261.

25) Kristián T, Pivovarova NB, Fiskum G, Andrews SB. Calcium-induced precipitate formation in brain mitochondria: composition, calcium capacity, and retention. *J Neurochem* 2007; **102**: 1346-1356.

26) Kokoszka JE, Waymire KG, Levy SE, Sligh JE, Cai J, Jones DP, et al. The ADP/ATP translocator is not essential for the mitochondrial permeability transition pore. *Nature* 2004; **427**: 461-465.

27) Gizatullina ZZ, Chen Y, Zierz S, Gellerich FN. Effects of extramitochondrial ADP on permeability transition of mouse liver mitochondria. *Biochim Biophys Acta* 2005; **1706**: 98-104.

28) Kristián T, Gertsch J, Bates TE, Siesjö BK. Characteristics of the calcium-triggered mitochondrial permeability transition in nonsynaptic brain mitochondria: effect of cyclosporin A and ubiquinone O. *J Neurochem* 2000; **74**: 1999-2009.

29) Chen JS, Chen KT, Fan CW, Han CL, Chen YJ, Yu JS, et al. Comparison of membrane fraction proteomic profiles of normal and cancerous human colorectal tissues with gel-assisted digestion and iTRAQ labeling mass spectrometry. *FEBS J* 2010; **277**: 3028-3038.

30) Chen YW, Chou HC, Lyu PC, Yin HS, Huang FL, Chang WS, et al. Mitochondrial proteomics analysis of tumorigenic and metastatic breast cancer markers. *Funct Integr Genomics* 2011; **11**: 225-239.

31) Fountoulakis M, Schlaeger EJ. The mitochondrial proteins of the neuroblastoma cell line IMR-32. *Electrophoresis* 2003; **24**: 260-275.

32) Pinton P, Ferrari D, Rapizzi E, Di Virgilio F, Pozzan T, Rizzuto R. The Ca^{2+} concentration of the endoplasmic reticulum is a key determinant of ceramide-induced apoptosis: significance for the molecular mechanism of Bcl-2 action. *EMBO J* 2001; **20**: 2690-2701.

33) Roy SS, Madesh M, Davies E, Antonsson B, Danial N, Hajnóczky G. Bad targets the permeability transition pore independent of Bax or Bak to switch between Ca2+-dependent cell survival and death. *Mol Cell* 2009; **33**: 377-388.

34) Hagen T, Lagace CJ, Modica-Napolitano JS, Aprille JR. Permeability transition in rat liver mitochondria is modulated by the ATP-Mg/Pi carrier. *Am J Physiol Gastrointest Liver Physiol* 2003; **285**: G274-281.

35) Chinopoulos C, Adam-Vizi V. Mitochondrial Ca(2+) sequestration and precipitation revisited. *FEBS J* 2010; **277**: 3637-3651.

36) Weinbach EC, von Brand T. The isolation and composition of dense granules from Ca++-loaded mitochondria. *Biochem Biophys Res Commun* 1965; **19**: 133-137.

37) Becker GL, Chen CH, Greenawalt JW, Lehninger AL. Calcium phosphate granules in the hepatopancreas of the blue crab Callinectes sapidus. *J Cell Biol* 1974; **61**: 316-326.

38) Pivovarova NB, Andrews SB. Calcium-dependent mitochondrial function and dysfunction in neurons. *FEBS J* 2010; **277**: 3622-3636.

39) Hosokawa T, Saito T, Asada A, Fukunaga K, Hisanaga S. Quantitative measurement of in vivo phosphorylation states of Cdk5 activator p35 by Phos-tag SDS-PAGE. *Mol Cell Proteomics* 2010; **9**:1133-1143.

40) Uhlén M, Björling E, Agaton C, Szigyarto CA, Amini B, Andersen E, et al. A human protein atlas for normal and cancer tissues based on antibody proteomics. *Mol Cell Proteomics* 2005; **4**: 1920-1932.

FIGURE LEGENDS

Fig. 1. Expression of SCaMC isoforms in normal and tumour tissues. Generation of SCaMC-1-KD cell lines.

A) Immunoblot analysis of SCaMC-1 and SCaMC-3 expression in total homogenates from mouse tissues and from COS-7 and 143B cells. Antibodies against Hsp60 were used as loading control. B: Brain; L: Liver; FL: fetal liver; S: spleen; K: kidney; H: heart; C: colon; SI: small intestine; LU: lung; M: muscle; T: testis; WF: white fat; BF: brown fat. **B)** Disease summary for SCaMC family (SCaMC-1, SCaMC-2, SCaMC-3) analysed by the Oncomine database (www.oncomine.org). Table shows the number of significant unique analyses across the whole oncomine database (including 93 datasets curated for *cancer vs.normal* analysis) with overexpression (red) or underexpression (blue). Cell color is determined by the best gene rank percentile for the analyses within the cell. SCaMC-1 shows overexpression/underexpression ratio of 67/33 from 192 analyses, in contrast to 14/28 from 125 and 19/65 from 165 for SCaMC-2 and SCaMC-3, respectively. A threshold significance value of 0.05 was used including setting to 'ALL' for fold change, gene rank thresholds and data types. For links to the analyses see supplementary text. Right panel: Comparison of SCaMC-1/SLC25A24 expression across 67 cancer vs. normal analyses including over-expression (mRNA) and copy number gain (DNA). The rank for a gene is the median rank for that gene across each of the analyses. The p-Value of the median-ranked analysis is shown. For references and link to analysis see supplementary text. **C**) Protein expression profiles of SCaMC-1 (upper panel) and SCaMC-2 (lower panel) obtained in the Human Protein Atlas database (www.proteinatlas.org) based on immunohistochemistry on cancer samples.[40] The color determines the percentage of cancer samples in the database with a given expression level. SCaMC-3 is not available in the database. **D-F**) Immunoblot to detect SCaMC-1 and other SCaMC isoforms in total homogenates (**D**) or isolated mitochondria (**E**) from COS-7 and 143B control (C) and SCaMC-1-KD (KD) cells. Mouse brain (B) and liver (L) mitochondria are also shown in (**E**). Antibodies against Hsp60, GAPDH or CyP-D were used as loading control. **F**) Quantification of the expression of SCaMC-1 or Hsp60 compared to GAPDH (mean ± SEM, n=5). **G**) Immunofluorescence in COS-7 and 143B control and SCaMC-1-KD cells using anti-SCaMC-1 antibodies.

Fig. 2. Ca^{2+}-dependent/CAT-insensitive adenine nucleotide uptake through SCaMC-1.

(A-C) 143B cells transiently expressing mitochondrial luciferase[17] were permeabilized and 100 μM luciferin was added to report mitochondrial ATP levels. Black traces indicate control cells, whereas red traces show SCaMC-1-KD cells. **A**) ANT activity in the absence of Ca^{2+}: the medium contained 100 μM EGTA, and 1 mM ATP was added when indicated. The traces marked with arrows were obtained from cells treated with 10 μM CAT. **B-C**) SCaMC-1

activity: the medium contained 100 μM Ca^{2+} and 10 μM CAT, and 1 mM ATP (**B**) or 2 mM ADP (**C**) were added when indicated. Bar charts indicate transport rate of SCaMC-1-KD (*KD*) cells compared to controls (C) (mean ± SEM, n=6).

(**D-F)** To determine the Ca^{2+} sensitivity of SCaMC-1 mediated ATP/ADP transport, mitochondrial ATP changes were measured in isolated mitochondria from COS-7 cells stably expressing mitochondrial luciferase after addition of 100 μM luciferin. **D)** The medium contained 10 μM CAT and free Ca^{2+} at the indicated concentrations, and 1 mM ATP was added when indicated. **E**) Efflux of ATP from mitochondria was triggered with the addition of 10 mM Pi followed by different Ca^{2+} concentrations. The efflux was reverted at the end of the experiment by addition of 1 mM ADP. **F**) Ca^{2+} activation of CAT-insensitive ATP transport. Transport rates were calculated from the slopes in panel **D** after ATP addition and fit to the equation: $V = V_0 + [(V_{max} - V_0) \times [Ca^{2+}]^N) / (S_{0.5}{}^N + [Ca^{2+}]^N)]$ (where V is transport activity at each $[Ca^{2+}]$, V_0 is the basal transport rate at $[Ca^{2+}] \approx 0$, V_{max} is the maximal activity, N is the hill coefficient and $S_{0.5}$ is the Ca^{2+} concentration which generates half-maximal transport activity). Pooled data of 6 independent experiments are shown.

Fig. 3. SCaMC-1 selectively protects from oxidative stress induced cell death.

A) Left panel: Control and SCaMC-1-KD 143B cells were incubated with H_2O_2 for 6 h and cell death was evaluated by confocal microscopy after 1 μM Calcein-AM and 2 μM PI staining. Right panel: Control and SCaMC-1-KD COS-7 cells were incubated with menadione for 2 hours and cell death was evaluated by flow cytometry after PI staining (Mean ± SEM, n= 6 and 5, respectively. * $p < 0.05$) **B**) Control and SCaMC-1-KD 143B cells were incubated with 1 mM H_2O_2 for 3.5 h or with 100 μM menadione for 1 h and cell death was evaluated by flow cytometry after TMRM and annexin V-FITC staining. A representative experiment is shown where **H** indicates the percentage of healthy cells (positive for TMRM and negative for annexin V, delimited by the quadrant), **D** indicates the percentage of dead cells (negative for TMRM and positive for annexin V). The number at the bottom of each panel indicates the percentage (mean ± SEM, n=6) of healthy cells. **$p = 0.00031$. *$p = 0.014$. **C**) Control and SCaMC-1-KD COS-7 and 143B cells are equally sensitive to 1 μM staurosporine induced cell death. Cells were treated with the drug for 0, 16 or 40 h and death was evaluated by flow cytometry after PI and annexin V-FITC staining. **D**) SCaMC-1-KD cells are more vulnerable to phototoxicity-induced oxidative stress. Control and SCaMC-1-KD COS-7 cells were loaded with 100 nM TMRM, illuminated with 10% laser power of the 543 nm HeNe line of the confocal system and the collapse of the mitochondrial $\Delta\Psi$ was monitored over time. Lower left panels: SCaMC-1-KD cells were treated with 100 μM EGTA and 1 μM thapsigargin. Lower right panels: cell treated with 5 μM CsA and 50 μM BKA. Figure shows representative images of at least 3 independent

experiments. **E**) Sensitivity to mPT dependent cell death of SCaMC-1 overexpressing 143B SCaMC-1-KD cells (left panel) and liver clone 9 cells (right panel). Cells were transiently transfected with GFP, or with GFP and SCaMC-1 and exposed to C_2 ceramide or H_2O_2 for 6 hours. The graph bar shows the change in percentage of GFP fluorescent cells (as compared to total cell number) after the treatment.[21] An increase in this percentage compared with control transfections indicates protection by SCaMC-1. The right panel shows the increase in SCaMC-1 expression after the transfection. SCaMC-1*: rescue construct with synonymous mutations (see the Supplementary Methods section). **F**) Control and stable SCaMC-1 overexpresing liver clone 9 cells were incubated with H_2O_2 for 3 h and cell death was evaluated by flow cytometry after PI staining (Mean ± SEM, n= 3. * $p < 0.05$). The right panel shows the increase in SCaMC-1 expression in the stable SCaMC-1 overexpressing clone.

Fig. 4. SCaMC-1 *knock-down* reduces mitochondrial Ca^{2+} buffering in intact cells and isolated mitochondria.

Agonist induced Ca^{2+} rises in cytosol (**A**) and mitochondria (**B**) of cells transiently expressing cytAEQ and mtAEQwt probes, respectively. Ca^{2+} signals were induced by ATP in COS-7 and by histamine in 143B cells (black: controls, red: SCaMC-1-KD). Bar charts show the quantification of the results in control (C) and SCaMC-1-KD cells (KD, mean ± SEM, n=3). **C**) Mitochondrial [Ca^{2+}] of COS-7 (left panel) and 143B (right panel) permeabilized cells after addition of 10 μM (free [Ca^{2+}]) Ca^{2+} to the IC buffer. Bar charts show the quantification of the results in control (C) and SCaMC-1-KD cells (KD, mean ± SEM, n=3). **D)** Ca^{2+} uptake rate in permeabilized cell and isolated mitochondria, measured by Calcium Green 5N free salt as an extramitochondrial Ca^{2+} indicator**.** A 20 μM (free [Ca^{2+}]) Ca^{2+} pulse was added where indicated (black: controls, red: SCaMC-1-KD). **E**) Ca^{2+} efflux was measured using Calcium Green 5N free salt in the extramitochondrial space of isolated 143B mitochondria, in the presence of 1 mM ATP, followed by loading with 320 nmol of Ca^{2+} per mg of protein. Where indicated, 200 nM RR was added to inhibit Ca^{2+} uptake, followed by the addition of 10 mM NaCl to stimulate the Na^+/Ca^{2+} exchanger (black: controls, red: SCaMC-1-KD). Bar chart shows the quantification of Na^+-independent (white bars) and Na^+-dependent (black bars) Ca^{2+} efflux rates in control and SCaMC-1-KD mitochondria (mean ± SEM, n=3 * $p < 0.05$).

Fig. 5. SCaMC-1 reduces Ca^{2+} sensitivity of mPT in isolated mitochondria and permeabilized cells.

Ca^{2+} mediated mPT in control (black traces) and SCaMC-1-KD (red traces) COS-7 **(A-B,D)** and 143B cell **(C,E)** mitochondria.

A) Quantification of Ca^{2+} retention capacity after administration of subsequent Ca^{2+} pulses (20 μM each) to control (white bars) and SCaMC-1-KD (black bars) permeabilized COS-7 cells

(0.15 mg total protein/mL). CRC was determined in the presence or absence of adenine nucleotides, Mg^{2+} and inhibitors. The Ca^{2+} concentration required to open the mPTP is shown. (mean ± SEM, n=6-16)

B,C) CRC was measured in isolated mitochondria in the presence of 1 mM ATP (**B**) or 2 mM ADP (**C**) using the Ca^{2+} sensitive probe Calcium Green 5N free salt in the extramitochondrial space. Experiments started by the addition of mitochondria, followed by repetitive Ca^{2+} pulses (arrows, 20 μM each). The traces marked with a long arrow are in the presence of 5 μM CsA.

D,E) Swelling of isolated mitochondria after subsequent Ca^{2+} pulses (arrows, 40 μM each) was measured as a decrease in light scattering at an absorbance of 540 nm in the presence (left panel) or absence (middle panel) of 2 mM ATP. Traces in the right panel were recorded in the presence of 2 mM ATP and either 5 μM CsA (**D**) or 200 nM RR (**E**).

F) The ERK pathway is constitutively active in 143B cells, but not in COS-7 cells and controls CyP-D phosphorylation. Left panels: Immunoblot against phospho- and total ERK, and phospho- and total GSK-3β in total homogenates from COS-7 and 143B cells. Right panel: Immunoblot against CyP-D in total homogenates from control or FLAG-CyP-D[8] overexpressing COS-7 and 143B cells after Mn^{2+}-Phos-tag SDS-PAGE.[39] Phosphorylated proteins are shifted upwards in the gel compared to unphosphorylated proteins. The same bands were observed when anti-FLAG antibodies were used, confirming the specificity of the bands (not shown). CyP-D phosphorylation is greatly decreased if the extracts are treated with alkaline phosphatase (AP) for 30 minutes (far right lane).

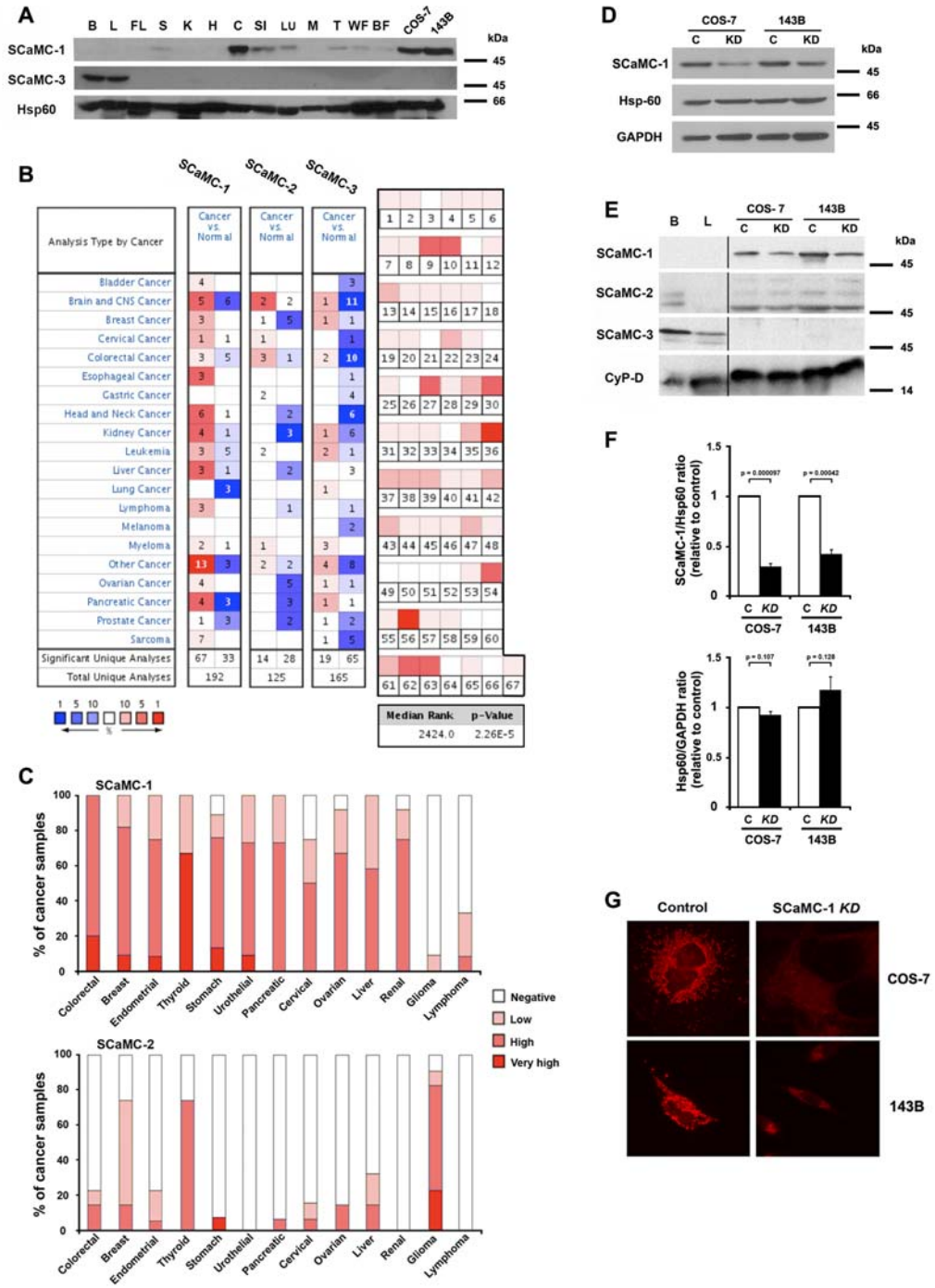
A
B L FL S K H C SI LU M T WF BF COS-7 143B
kDa
SCaMC-1
SCaMC-3
Hsp60
45
45
66
B
SCaMC-1
SCaMC-2
SCaMC-3
Analysis Type by Cancer
Cancer vs. Normal
Bladder Cancer
Brain and CNS Cancer
Breast Cancer
Cervical Cancer
Colorectal Cancer
Esophageal Cancer
Gastric Cancer
Head and Neck Cancer
Kidney Cancer
Leukemia
Liver Cancer
Lung Cancer
Lymphoma
Melanoma
Myeloma
Other Cancer
Ovarian Cancer
Pancreatic Cancer
Prostate Cancer
Sarcoma
Significant Unique Analyses
Total Unique Analyses
67 33
192
14 28
125
19 65
165
Median Rank
p-Value
2424.0
2.26E-5
C
SCaMC-1
% of cancer samples
Colorectal
Breast
Endometrial
Thyroid
Stomach
Urothelial
Pancreatic
Cervical
Ovarian
Liver
Renal
Glioma
Lymphoma
Negative
Low
High
Very high
SCaMC-2
D
COS-7
143B
C
KD
SCaMC-1
Hsp-60
GAPDH
E
B
L
SCaMC-1
SCaMC-2
SCaMC-3
CyP-D
14
F
SCaMC-1/Hsp60 ratio (relative to control)
Hsp60/GAPDH ratio (relative to control)
G
Control
SCaMC-1 KD
COS-7
143B

Fig 1

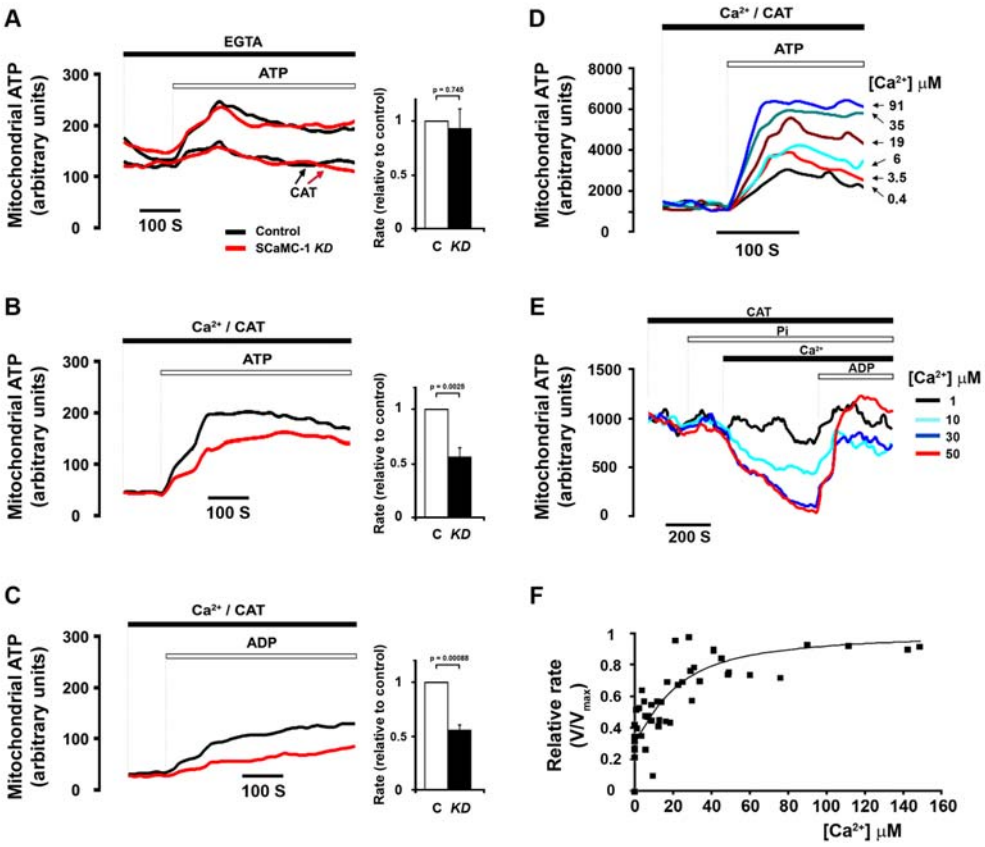
A
EGTA
ATP
Mitochondrial ATP (arbitrary units)
300
200
100
0
100 S
CAT
Control
SCaMC-1 KD
Rate (relative to control)
p = 0.745
1
0.5
0
C KD
B
Ca2+ / CAT
ATP
100 S
p = 0.0025
C KD
C
Ca2+ / CAT
ADP
100 S
p = 0.00068
C KD
D
Ca2+ / CAT
ATP
8000
6000
4000
2000
0
100 S
[Ca2+] μM
91
35
19
6
3.5
0.4
E
CAT
Pi
Ca2+
ADP
1500
1000
500
0
200 S
[Ca2+] μM
1
10
30
50
F
Relative rate (V/Vmax)
1
0.8
0.6
0.4
0.2
0
0 20 40 60 80 100 120 140 160
[Ca2+] μM

Fig 2

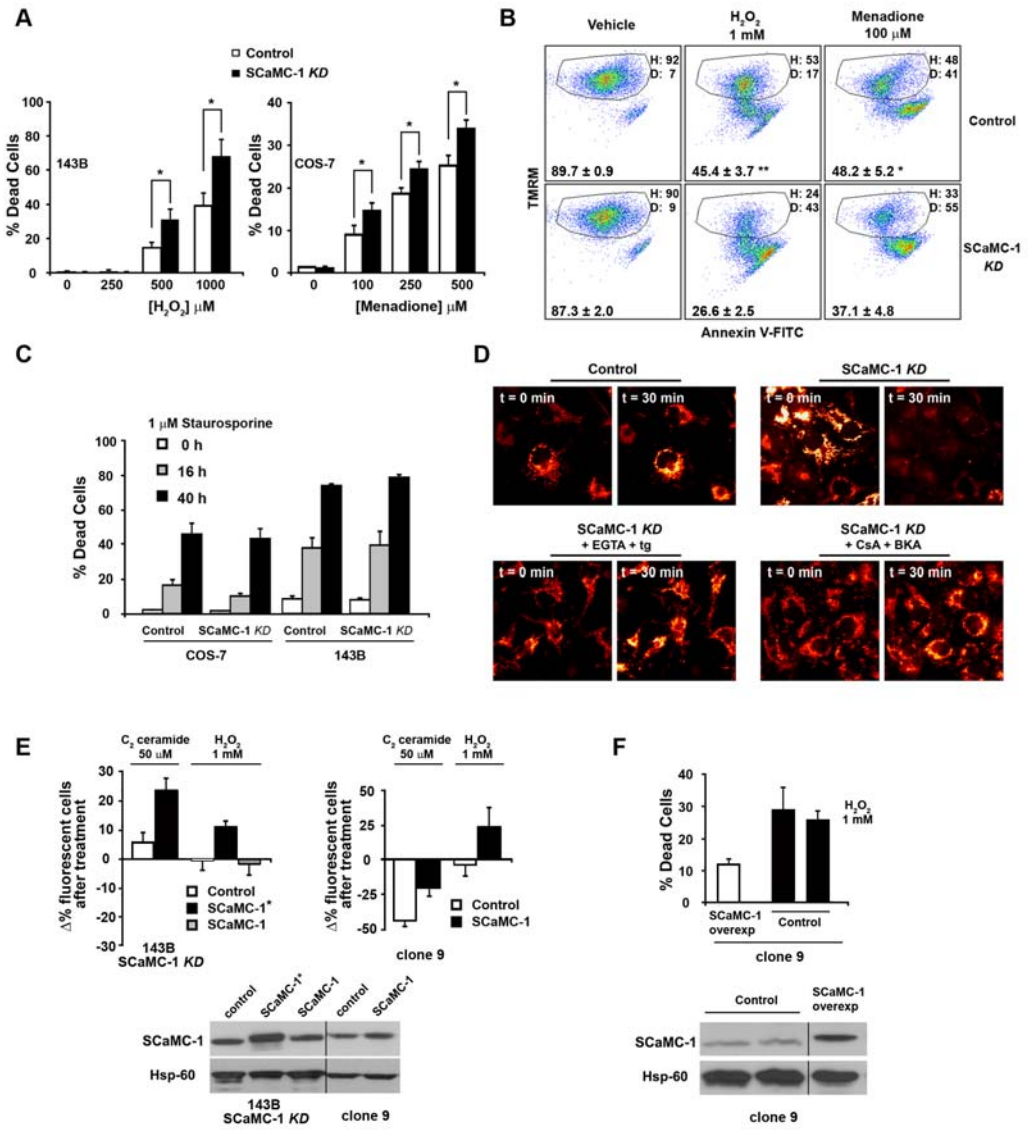
A
Control
SCaMC-1 KD
% Dead Cells
143B
COS-7
[H2O2] μM
[Menadione] μM
B
Vehicle
H2O2 1 mM
Menadione 100 μM
H: 92 D: 7
89.7 ± 0.9
H: 53 D: 17
45.4 ± 3.7 **
H: 48 D: 41
48.2 ± 5.2 *
H: 90 D: 9
87.3 ± 2.0
H: 24 D: 43
26.6 ± 2.5
H: 33 D: 55
37.1 ± 4.8
TMRM
Annexin V-FITC
Control
SCaMC-1 KD
C
1 μM Staurosporine
0 h
16 h
40 h
% Dead Cells
Control
SCaMC-1 KD
COS-7
143B
D
Control
SCaMC-1 KD
t = 0 min
t = 30 min
SCaMC-1 KD + EGTA + tg
SCaMC-1 KD + CsA + BKA
E
C2 ceramide 50 μM
H2O2 1 mM
Δ% fluorescent cells after treatment
Control
SCaMC-1*
SCaMC-1
143B SCaMC-1 KD
clone 9
control
SCaMC-1*
SCaMC-1
SCaMC-1
Hsp-60
F
% Dead Cells
H2O2 1 mM
SCaMC-1 overexp
Control
clone 9
SCaMC-1 overexp

Fig 3

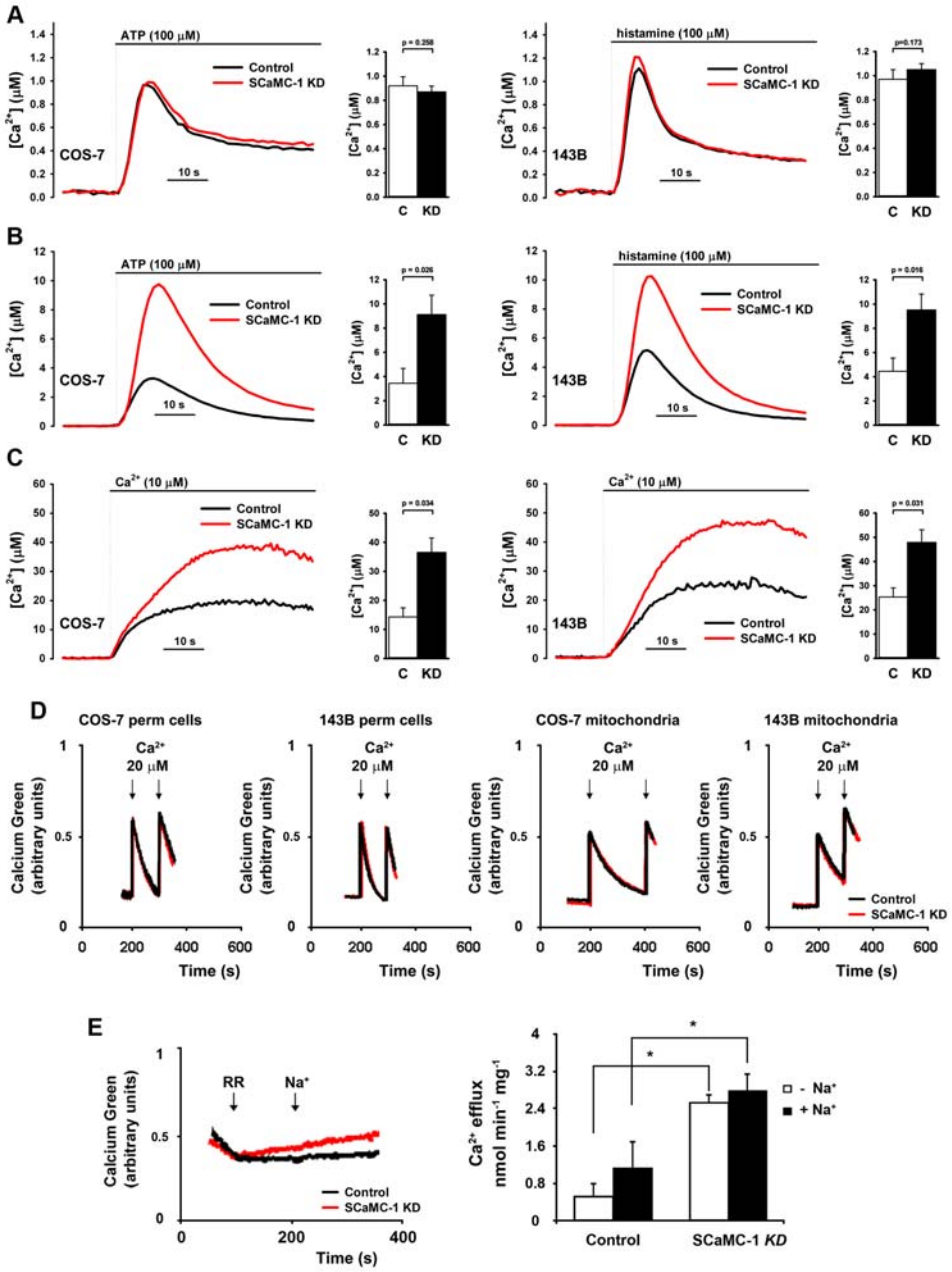
A
ATP (100 μM)
Control
SCaMC-1 KD
COS-7
10 s
[Ca2+] (μM)
C KD
histamine (100 μM)
143B
B
C
Ca2+ (10 μM)
D
COS-7 perm cells
143B perm cells
COS-7 mitochondria
143B mitochondria
Ca2+
20 μM
Calcium Green (arbitrary units)
Time (s)
E
RR
Na+
Ca2+ efflux nmol min-1 mg-1
- Na+
+ Na+
Control
SCaMC-1 KD

Fig 4

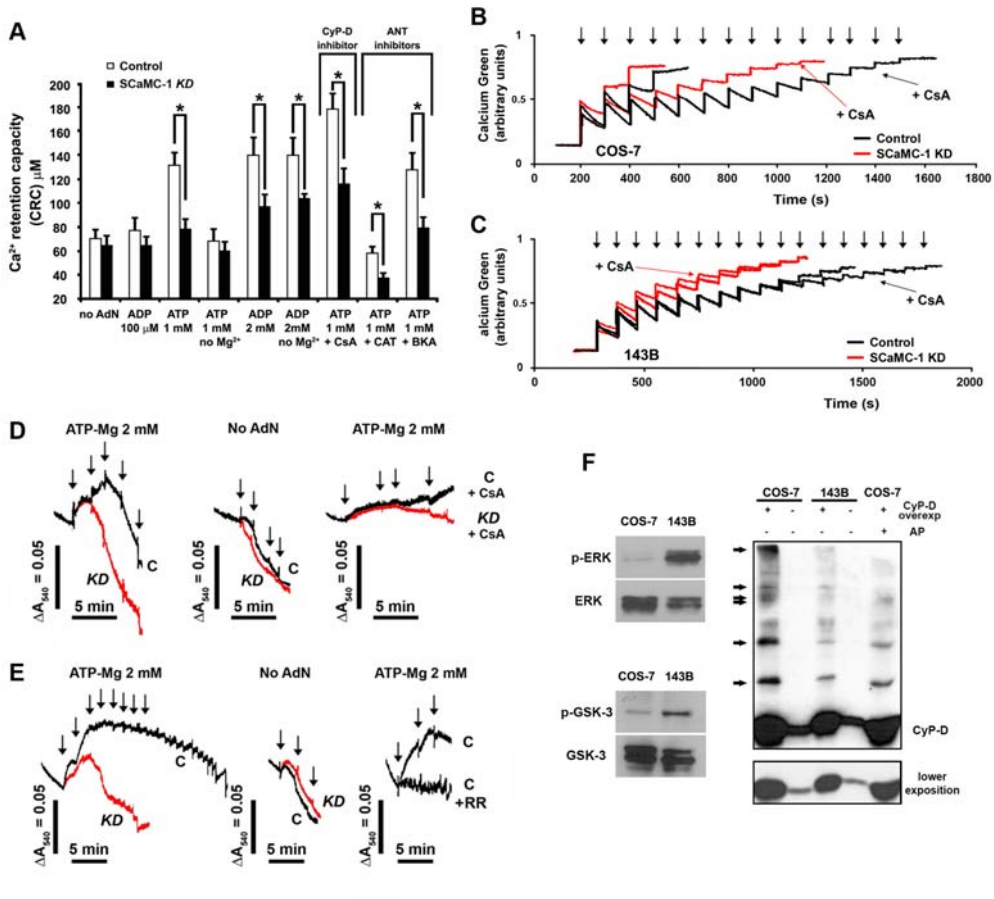
A
Control
SCaMC-1 KD
CyP-D inhibitor
ANT inhibitors
Ca2+ retention capacity (CRC) µM
no AdN
ADP 100 µM
ATP 1 mM
ATP 1 mM no Mg2+
ADP 2 mM
ADP 2mM no Mg2+
ATP 1 mM + CsA
ATP 1 mM + CAT
ATP 1 mM + BKA
B
Calcium Green (arbitrary units)
+ CsA
COS-7
Control
SCaMC-1 KD
Time (s)
C
alcium Green (arbitrary units)
143B
D
ATP-Mg 2 mM
No AdN
C
+ CsA
KD
5 min
E
+RR
F
COS-7
143B
p-ERK
ERK
p-GSK-3
GSK-3
CyP-D overexp
AP
CyP-D
lower exposition

Fig 5

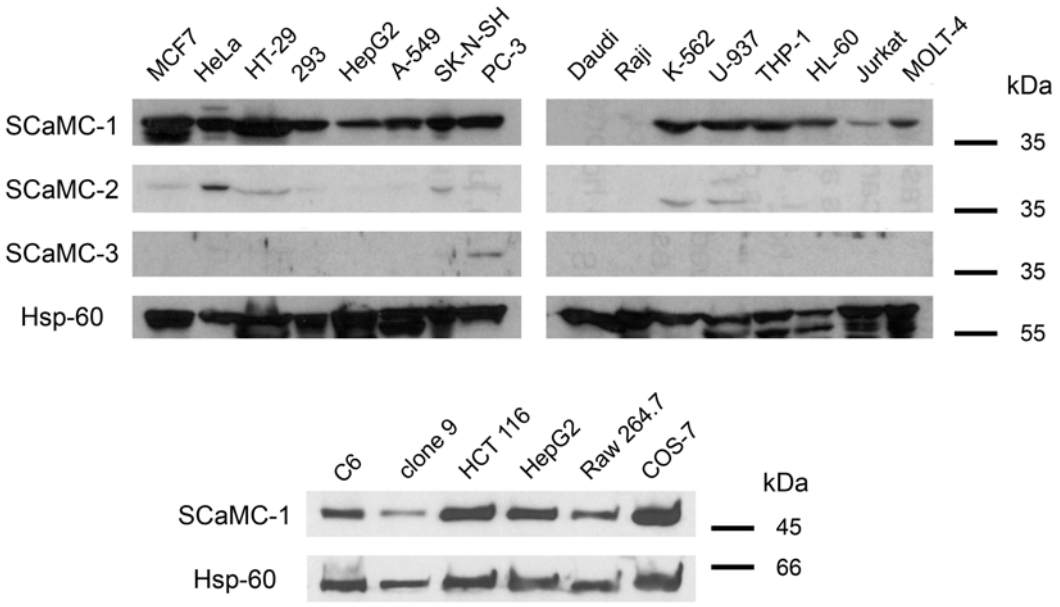
MCF7
HeLa
HT-29
293
HepG2
A-549
SK-N-SH
PC-3
Daudi
Raji
K-562
U-937
THP-1
HL-60
Jurkat
MOLT-4
kDa
SCaMC-1
SCaMC-2
SCaMC-3
Hsp-60
35
35
35
55
C6
clone 9
HCT 116
HepG2
Raw 264.7
COS-7
kDa
SCaMC-1
Hsp-60
45
66

Fig S1

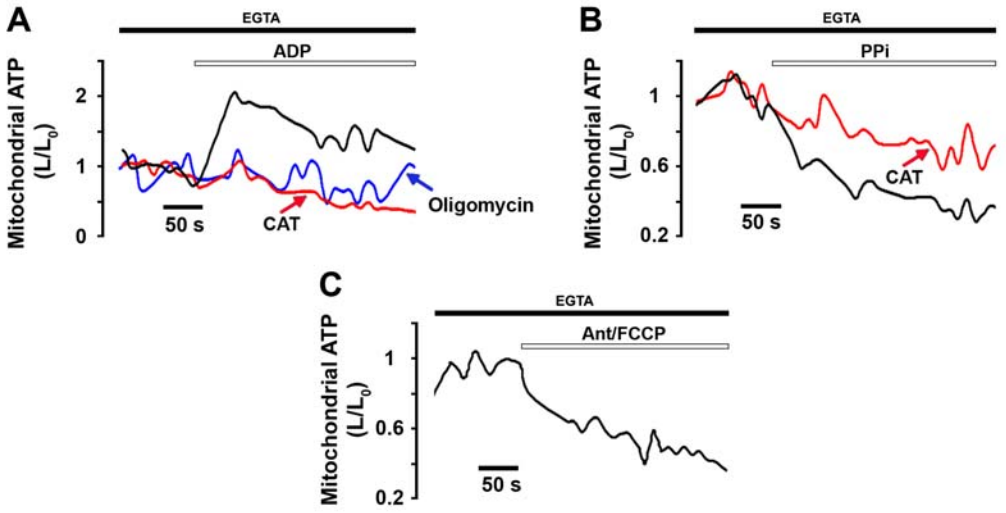
A
EGTA
ADP
Mitochondrial ATP
(L/L0)
2
1
0
50 s
CAT
Oligomycin
B
EGTA
PPi
Mitochondrial ATP
(L/L0)
1
0.6
0.2
CAT
50 s
C
EGTA
Ant/FCCP
Mitochondrial ATP
(L/L0)
1
0.6
0.2
50 s

Fig S2

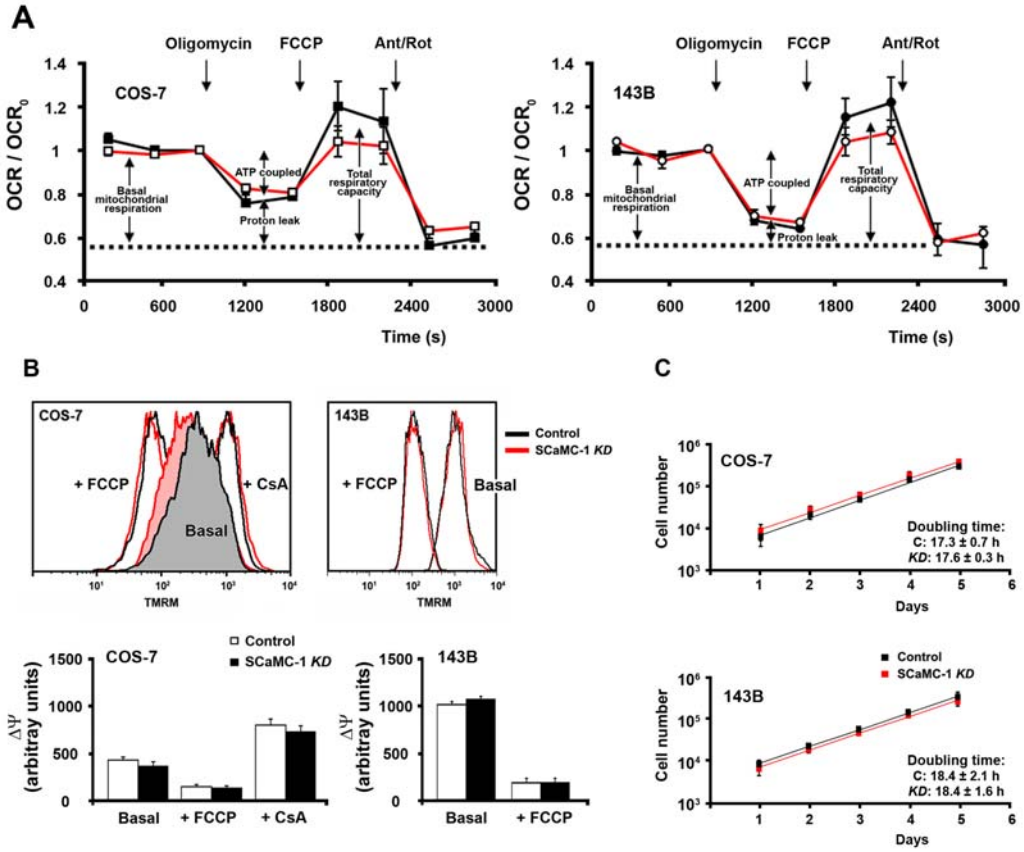
A
Oligomycin
FCCP
Ant/Rot
COS-7
143B
OCR / OCR0
Basal mitochondrial respiration
ATP coupled
Proton leak
Total respiratory capacity
Time (s)
B
COS-7
143B
+ FCCP
+ CsA
Basal
TMRM
Control
SCaMC-1 KD
ΔΨ (arbitray units)
C
Cell number
Doubling time:
C: 17.3 ± 0.7 h
KD: 17.6 ± 0.3 h
Doubling time:
C: 18.4 ± 2.1 h
KD: 18.4 ± 1.6 h
Days

Fig S3

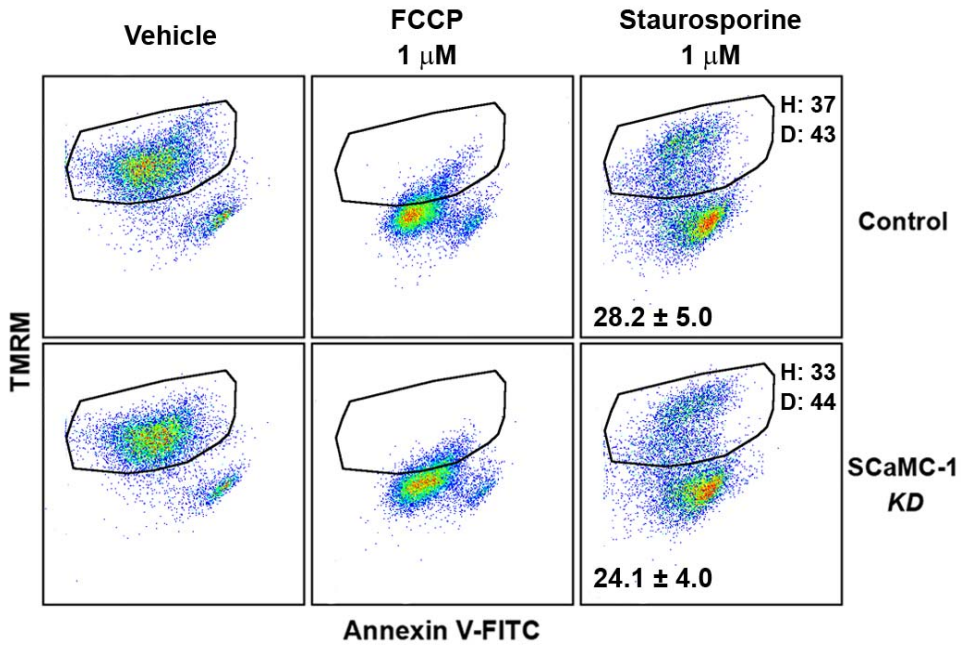
Vehicle
FCCP
1 μM
Staurosporine
1 μM
H: 37
D: 43
Control
28.2 ± 5.0
H: 33
D: 44
SCaMC-1
KD
24.1 ± 4.0
TMRM
Annexin V-FITC

Fig S4

	COS-7		143B	
	Control	*KD*	Control	*KD*
Total OCR	103.5 ± 9.0	107.5 ± 14.9	182.4 ± 37.5	161.0 ± 38.5
A) Non-mitochondrial OCR	55.1 ± 4.9	66.5 ± 11.1	114.1 ± 39.2	92.9 ± 29.7
B) Mitochondrial OCR	48.4 ± 5.2	40.9 ± 5.2	68.3 ± 2.0	68.2 ± 9.2
- ATP coupled	50 ± 4 % (24.8 ± 4.7)	48 ± 3 % (19.6 ± 2.5)	83 ± 10 % (58.6 ± 7.0)	73 ± 4 % (51.0 ± 10.2)
- Proton leak	50 ± 4 % (23.6 ± 1.9)	52 ± 3 % (21.3 ± 3.0)	17 ± 9 % (9.6 ± 9.0)	27 ± 4 % (17.1 ± 1.5)
Total respiratory capacity	56.8 ± 11.2	48.4 ± 10.3	97.0 ± 24.2	75.6 ± 5.8

Table S1